UC San Diego

UC San Diego Previously Published Works

Title

Geographically resolved social cost of anthropogenic emissions accounting for both direct and climate-mediated effects

Permalink

https://escholarship.org/uc/item/37b9048c

Journal

Science Advances, 8(38)

ISSN

2375-2548

Authors

Burney, Jennifer
Persad, Geeta
Proctor, Jonathan
et al.

Publication Date

2022-09-23

DOI

10.1126/sciadv.abn7307

Peer reviewed

eScholarship.org Powered by the California Digital Library
University of California

ATMOSPHERIC SCIENCE

Geographically resolved social cost of anthropogenic emissions accounting for both direct and climate-mediated effects

Jennifer Burney[1]*†, Geeta Persad[2]*†, Jonathan Proctor[3], Eran Bendavid[4], Marshall Burke[5], Sam Heft-Neal[6]

Copyright © 2022 The Authors, some rights reserved; exclusive licensee American Association for the Advancement of Science. No claim to original U.S. Government Works. Distributed under a Creative Commons Attribution NonCommercial License 4.0 (CC BY-NC).

The magnitude and distribution of physical and societal impacts from long-lived greenhouse gases are insensitive to the emission source location; the same is not true for major coemitted short-lived pollutants such as aerosols. Here, we combine novel global climate model simulations with established response functions to show that a given aerosol emission from different regions produces divergent air quality and climate changes and associated human system impacts, both locally and globally. The marginal global damages to infant mortality, crop productivity, and economic growth from aerosol emissions and their climate effects differ by more than an order of magnitude depending on source region, with certain regions creating global external climate changes and impacts much larger than those felt locally. The complex distributions of aerosol-driven societal impacts emerge from geographically distinct and region-specific aerosol-climate interactions, estimation of which is enabled by the full Earth System Modeling Framework used here.

INTRODUCTION

Credible climate accounting—or the valuation of impacts from anthropogenic emissions—requires linking emissions from known sources to their downstream benefits and damages. A robust literature has emerged to estimate the social cost of carbon (SCC) or the marginal damages associated with an additional emission of carbon dioxide (CO_2) (*1*–*5*). Development of the SCC methodology has benefited from the physical reality that CO_2 is long lived and well mixed in the atmosphere, and its impacts on the Earth system are thus independent of emission location. Along with CO_2, however, human activities also produce coemissions of shorter-lived compounds—including black carbon (BC) and organic carbon (OC) aerosols, carbon monoxide, nitrogen oxides, volatile organic compounds, sulfur dioxide (SO_2), and other trace chemicals—that are not well mixed and thus likely exert geographically heterogeneous influence on atmospheric composition, climate, and human systems (*6*–*8*). A full cost-benefit analysis of any mitigation action or policy would ideally take into account the emission location and balance the cost of mitigation against the full suite of benefits that would accrue from all mitigated coemissions, in addition to CO_2.

Although the idea of accounting for these cobenefits is not new (*9*–*14*), geographically resolved climate accounting that includes the effects of short-lived pollutants has yet to be implemented, because it requires tracing both the air quality and climate impacts of identical emissions from different locations. Previous studies have either focused only on air quality-related health impacts (*15*–*17*), assessed emissions from a single region (*18*–*20*), used simplified models without coupled chemistry and climate (*17*, *21*–*26*), or have modeled emissions reduction scenarios where emissions are simultaneously reduced across broad areas, which cannot isolate the full impact of an emission from a particular location (*27*–*30*). Building on recent literature on the spatial dependence of aerosol-climate interactions (*7*, *8*, *31*–*34*), here, we link novel aerosol perturbation experiments in a fully dynamical, global Earth system model with empirically estimated damage functions to map the per-emission size and spatial distribution of physical changes and societal damages that accrue from aerosols emitted by eight representative regions (Brazil, China, East Africa, Western Europe, India, Indonesia, the United States, and South Africa; fig. S1). This allows us to geographically resolve the marginal societal impacts of aerosol emissions from different regions, not only through their localized effects on air quality [i.e., surface concentrations of particulate matter with diameter <2.5 micrometers ($PM_{2.5}$) and column-integrated aerosol optical depth (AOD)] but also through their heterogeneous impacts on climate (i.e., temperature and precipitation) in an integrated framework. Many important outcomes are known to be multivariate functions of environmental exposures, and our results demonstrate that inclusion of geographically resolved climate pathways substantially modifies the estimation of societal impacts compared to prior approaches. By using a fully coupled Earth system model, our methodology allows us to assess, in a self-consistent manner, impacts due to changes across a range of environmental parameters that are all affected in spatially and temporally varying ways by the aerosols and their precursors that are coemitted with CO_2.

The analysis framework is shown in fig. S1. Briefly, we run the National Center for Atmospheric Research Community Atmosphere Model 5 (NCAR CAM5) model coupled to a slab ocean for 100 years with a repeating annual cycle of boundary conditions. In the control environment, global CO_2 concentrations are held at year 2000 levels, and aerosols are fixed at 1850 levels. In the perturbation environment, we separately impose an additional aerosol emissions burden generated in one of the eight regions (i.e., eight separate experimental conditions). This additional emissions burden is equal in

[1]School of Global Policy and Strategy, University of California, San Diego, CA, USA. [2]Department of Geological Sciences, University of Texas at Austin, Austin, TX, USA. [3]Center for the Environment and Data Science Initiative, Harvard University, Cambridge, MA, USA. [4]Department of Medicine, Stanford University, Stanford, CA, USA. [5]Department of Earth System Science, Stanford University, Stanford, CA, USA. [6]Center on Food Security and the Environment, Stanford University, Stanford, CA, USA.
*Corresponding author. Email: jburney@ucsd.edu (J.B.); geeta.persad@jsg.utexas.edu (G.P.)
†These authors contributed equally to this work.

magnitude and composition across experiments and includes a modern representative mix (roughly equivalent to year 2000 emissions in China) of BC, OC, and sulfate precursor (here SO_2), which is interactively transported, aged, and removed by the circulation and chemistry of the model. While other coemitted pollutants—including heavy metals, high Global Warming Potential (GWP) gases, and ozone precursors such as NOx, methane, and other volatile organic compounds—are known to contribute to secondary aerosol formation and to affect human health, plant health, and climates, BC, OC, and SO_2 drive the vast majority of non-greenhouse gas (GHG) climate effects (*35*) and are the main anthropogenic contributors to present-day $PM_{2.5}$ levels in most regions (*36*, *37*).

We then link the steady-state environmental changes in each experiment to established exposure-response functions from the literature to estimate impacts on infant mortality (due to surface $PM_{2.5}$ concentrations) (*38*), yields of main staple crops (due to changes in temperature, precipitation, and AOD; AOD is a measure of aerosol abundance in the full thickness of the atmosphere and influences the quantity and quality of light available for photosynthesis) (*39*), and macroeconomic growth (which shows a strong, nonlinear response to temperature) (*40*). While aerosols likely affect other important outcomes, both directly (e.g., adult morbidity and mortality) and indirectly (e.g., changes in soil moisture that lead to increased fire risk), we examine these three outcomes because they are key determinants of welfare and occur on annual or shorter time scales and are thus separable from longer-run aerosol (or GHG)–mediated processes. By holding the total quantity and composition of the emissions portfolio constant but varying its source location against an otherwise fixed-aerosol background, we test the extent to which a set of annual physical and societal impacts of this mix of BC + OC + SO_2 vary based on source location. To then scale these physically equivalent emissions scenarios to regionally representative conditions, we normalize to per-unit aerosol impacts and then normalize to regional CO_2 emissions to produce realistic coemissions impacts (see Methods for details). The first normalization allows us to assess the marginal damage per unit of aerosol emissions, and the second allows us to assess the marginal damage from coemitted aerosols per unit of CO_2 emissions. These marginal damages are the metrics used in the inventories and accounting systems that typically drive policy and provide a metric of damages from future incremental growth or mitigation of aerosol emissions in a given source region. Critically, we consider cobenefits and codamages that occur not only from air quality impacts but also from geographically resolved aerosol-induced climate changes.

RESULTS

Physical impacts including changes in surface $PM_{2.5}$, AOD, temperature, and precipitation differ substantially by emission region

We find a large divergence in impacts resulting from identical amounts of aerosols emitted from each source region that begins with strongly differing physical system responses under both air quality and climate conditions. After emission, primary BC and OC aerosols, as well as secondary sulfate aerosols formed from SO_2, are wafted into the atmosphere, transported, and deposited through a suite of mechanisms. Although the physical distribution of the particulates at the surface remains mostly local to the region of origin (Fig. 1A), higher up in the atmosphere aerosols are transported farther, resulting in increased aerosol optical depth locally and in downwind regions (Fig. 1B). These aerosols then exert radiative effects on climate by absorbing and scattering incoming radiation both directly and indirectly through cloud nucleation [see (*8*) for additional discussion]. This changes both the surface temperature and the temperature structure of the atmospheric column, which, in turn, affects larger-scale circulation patterns (Fig. 1C). Last, aerosols affect precipitation via changes to atmospheric stability and large-scale circulation and, potentially, through interactions with clouds as condensation nuclei (Fig. 1D).

Global-mean increases in surface $PM_{2.5}$ and column AOD from each region's emissions both vary by a factor of 2.5 (Fig. 1, A and B; fig. S2A; and table S1), symptomatic of differences in the removal

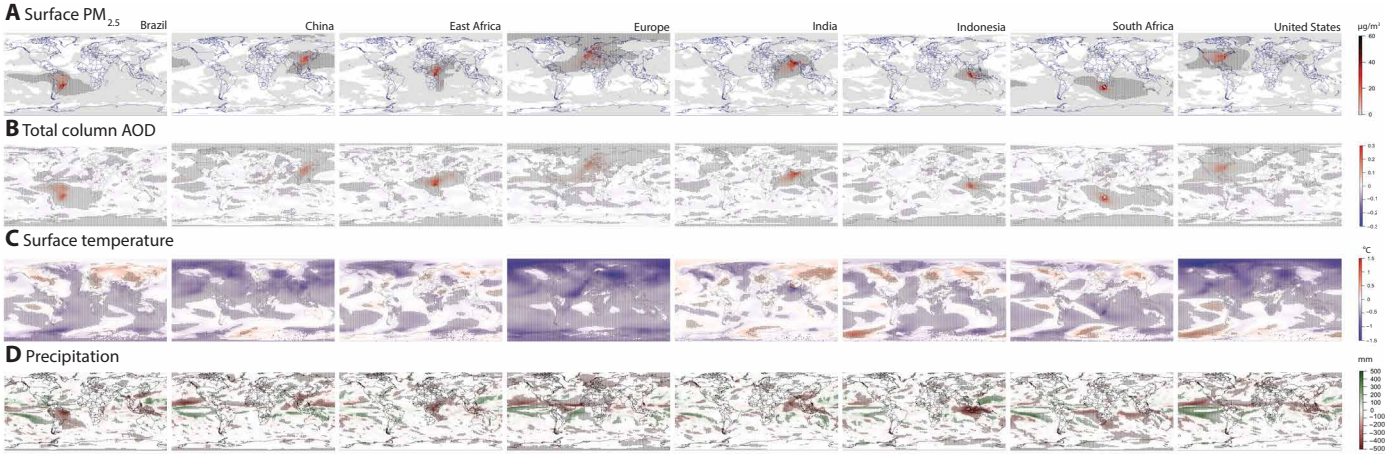

Fig. 1. Steady-state distributions of aerosols and their physical impacts relative to control condition. Each column shows the global impacts due to identical aerosol emissions from the listed region. (**A**) Changes in surface $PM_{2.5}$ show that the surface particulate burden remains concentrated locally, with different characteristic dispersion distances across regions; (**B**) changes in total column AOD span larger spatial scales; and (**C**) changes in average annual surface temperature show strong variation, with northern latitude emissions locations exerting the strongest global cooling impacts. (**D**) Average annual precipitation impacts are heterogeneous, with stronger reductions in the tropics. Stippling indicates a difference between perturbation from control conditions at the 95% confidence level.

processes and atmospheric transport patterns present in the ambient environment into which the aerosols are emitted (*41*, *42*). Global-mean surface temperature effects vary by more than an order of magnitude (Fig. 1C). Broadly, the distribution of the aerosols, the strength of regional radiative forcings produced, and the efficacy of the forcing at producing climate feedbacks all contribute to the magnified temperature differential relative to the surface $PM_{2.5}$ and column AOD differential (*8*). Global-mean total precipitation reductions vary by a factor of more than 6 (Fig. 1D) but are strongly correlated ($r = 0.95$) with the global-mean temperature response (fig. S2B) and can be viewed as a global hydrologic cycle response to the aerosol-induced cooling (*43*). The diversity of responses to identical emissions demonstrates that the geographic distribution of sources is a critical determinant of aerosols' influence on the physical environment.

Societal impacts differ by emission region and are driven by a combination of physical system changes and the spatial distribution of human systems

We evaluate three major welfare impacts—infant mortality, staple crop production, and gross domestic product (GDP)—that have been shown in studies of the recent past to respond to atmospheric changes on annual (or shorter) time scales. $PM_{2.5}$ in the surface air layer exposes infants both in utero and during infancy, which can increase the risk of respiratory infections (*44*), low birth weight (*45*), and neonatal mortality (*46*) (table S2). The net impact of AOD on photosynthetically available light (increasing diffuse but decreasing direct sunlight at the surface) reduces yields of maize, soy, rice, and wheat (*39*), while cooling and reduced precipitation during the growing season due to aerosols can either increase or decrease productivity depending on crop type and on baseline growing conditions relative to the optimum (table S3) (*47*). At a macroeconomic level, annual GDP growth has been shown to have a nonlinear response to temperature (table S4) (*40*). We quantify "global" (i.e., aggregated over the entire globe), "external" (i.e., aggregated only outside the aerosol source region), and "local" (i.e., aggregated only within the aerosol source region) impacts, such that global impacts are the sum of local and external impacts.

We find that the divergence in aerosol physical impacts based on emissions location leads to a divergence in societal impacts that is further magnified by the colocation of affected social systems and their underlying vulnerabilities. That is, the more spatial overlap between physical system changes and human systems and the more vulnerable the human system, the larger the social impact. The geographic distributions of cropped areas and human populations are shown in fig. S3A; their vulnerability is characterized by baseline conditions (infant mortality rate, baseline crop yields, and baseline per capita GDP), shown in fig. S3B. The influence of the colocation of physical changes and human systems is summarized in fig. S4, which shows how simple land area average, population-weighted average, and crop area–weighted average changes in $PM_{2.5}$, AOD, temperature, and precipitation can differ by up to a factor of 2 (e.g., local area average versus crop-weighted average precipitation for Indonesia, global average versus population-weighted infant mortality for Europe). We detail the impacts on infant mortality, crop productivity, and macroeconomics effects below.

The confluence of physical impact heterogeneity and the geography of human systems and vulnerabilities mean that global infant mortality impacts span almost two orders of magnitude across scenarios (Fig. 2, A and B, and fig. S5A)—a range 10-fold larger than the variation in surface $PM_{2.5}$ changes across the same scenarios. Aggregate crop productivity effects range from strongly negative to weakly positive (Fig. 2C and fig. S5B), as does GDP change (Fig. 2D and fig. S5C), although all source regions produce the same global-mean sign of change in the associated physical system drivers. (That is, global average temperature and precipitation are reduced, and global average AOD is increased, but localized crop productivity and economic growth impacts are mixed). Results are summarized in tables S5 and S6.

The degree of colocation of increased surface pollution with large vulnerable infant populations is the leading driver of disparities in excess infant deaths from the different source regions, as well as the degree to which impacts are felt locally versus globally (Fig. 2B and figs. S4 and S5A). Indian emissions produce the largest total atmospheric aerosol loadings (*8*) and, therefore, the largest increase in $PM_{2.5}$; this is strongly confined to the source region, likely due to the partial geographic barrier to ventilation created by the Himalayas. The spatial pattern of $PM_{2.5}$ increase is highly colocated with large, vulnerable infant populations as well, compounding with the large $PM_{2.5}$ increase to generate large infant mortality effects (fig. S3). The East African emissions experiment similarly produces a large number of excess infant deaths due to the colocation of the resulting surface pollution with large and highly vulnerable infant populations. European emissions do not produce as large of a total increase in $PM_{2.5}$, but the increase is spatially dispersed and colocated with external regions that have large, vulnerable infant populations. Combined with low infant vulnerability within Europe, this produces strongly externalized impacts—European emissions induce four times as many excess infant deaths outside regional boundaries than inside. The lower number of excess deaths from the U.S. emissions experiment emerges partially because the distribution of surface pollution produced is biased away from populated areas and infant numbers and because vulnerability is relatively low in the populated areas affected.

The spatial distribution of impacts on crop productivity stems from the distributions of the four crop types assessed (fig. S3), as well as their relative sensitivity to each of the three driving physical system changes (AOD, temperature, and precipitation) (table S3). In cases where crop productivity effects are of a different sign outside versus inside the source region (e.g., Europe and South Africa), the local AOD-driven reduction of photosynthetically available light dominates the crop response and generates large local crop productivity declines (Fig. 2C and figs. S4, S5B, and S6). In areas external to the source region, temperature and precipitation effects dominate the influence on crop productivity and may have either positive or negative impacts depending on the optimality of the baseline climate in that region for a given crop type. Wheat is the largest driver of overall productivity declines (fig. S6), amplified by the colocation of patterns of strong physical system change with wheat-growing regions in most of the experiment configurations.

Indian emissions again produce the largest negative global total crop impacts, but the global totals are largely driven by strong within-India (i.e., local) impacts. The same mechanisms that produce the large local surface $PM_{2.5}$ concentrations in response to Indian emissions contribute to enhance local AOD loading, which drives large absolute declines in the local production rate of all crop types, particularly wheat and rice (fig. S6). India has extensive area devoted to these crops, including some very high–yielding regions. Emissions from

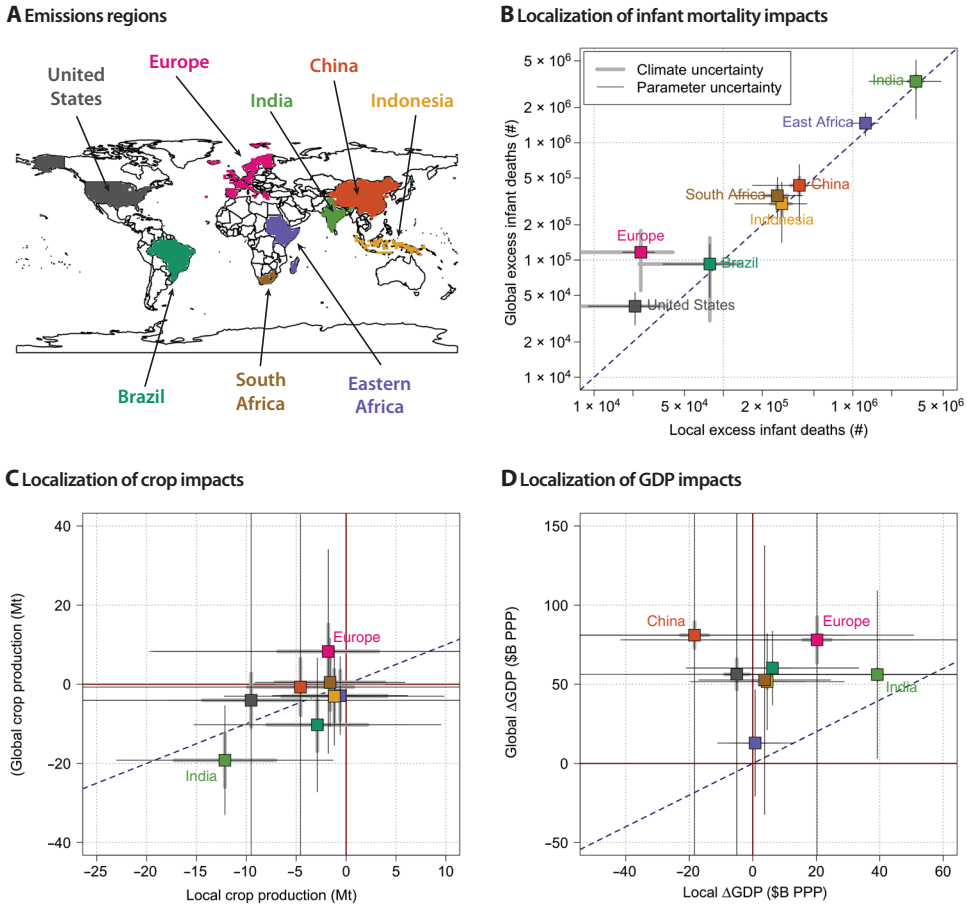

Fig. 2. The social impacts of aerosols from each source region. Each experimental condition compared equivalent aerosol emissions from one region (**A**) to control conditions; here, impacts are aggregated both locally (total within the emission region) and globally. Because the global total includes local impacts, location on the 1:1 line indicates purely localized impacts (local = global), while departures above or below the line indicate exported effects. (**B**) Excess infant deaths are large proximal to the source, although aerosol transport over populated and/or vulnerable regions creates distal impacts. (**C**) The geographic distribution of crop production changes varies widely, with heterogeneous radiation, temperature, and precipitation effects creating substantial distal impacts. (**D**) Economic impacts include both positive and negative effects, with positive impacts arising from cooling of countries above the economically optimal temperature under the control condition. Gray error bars show the uncertainty [95% confidence interval (CI)] due to natural climate variability present in simulations, and black bars show uncertainty (95% CI) from damage function parameter estimation. $B PPP, billions of dollars based on purchasing power parity (PPP). Point colors for (B) to (D) correspond to the emission regions colors in (A). Values are shown in table S5, and values normalized to per teragram (per-Tg) aerosol are shown in table S6.

Europe and South Africa damage local crop productivity while benefiting aggregate external crop productivity (Fig. 2C and fig. S5B). In these cases, aggregate external crop productivity is enhanced by the large-scale cooling generated by aerosols from these regions (fig. S6), which is more geographically dispersed than the increased AOD (Fig. 1). However, note that emission source locations with aggregate local crop benefits still cause discernible declines throughout northern Africa, the Middle East, and South Asia (fig. S5B).

The geographic distribution of macroeconomic effects (Fig. 2D and fig. S5C) bears the fingerprint of the nonlinear (inverted-U) influence of temperature on GDP (*40*). Because the aerosols cool globally regardless of source location, regions whose climatological temperature is above the economic optimum (e.g., India) experience cooling-driven economic benefits from their own emissions, while those with climatological temperature below or at the economic optimum (e.g., China and the United States) experience cooling-driven economic damages. An exception to this is Europe, driven by the fact that the large temperature changes induced by European emissions occur primarily outside of the source region. No source region generates net global aggregate damages, although all emission regions have important distal impacts (fig. S5C). We note that these calculations consider the influence of aerosol-driven changes in only temperature on GDP; effects of aerosol emissions on GDP through changes in particulate matter (*48*) or other climate variables such as rainfall (*49*) could potentially mitigate or enlarge aerosol-driven cooling benefits to GDP, although quantitative understanding of these aerosol-mediated effects is limited.

We explore the relative contributions of the physical changes, the geography of human systems, and their underlying vulnerability by comparing our simulations to highly idealized counterfactual scenarios in which either (i) the physical system changes are spatially homogeneous (held at the global mean change for each scenario), (ii) the spatial distributions of the affected system (infants, crops, and people) are homogeneous, or (iii) the spatial distribution of vulnerability is homogeneous (i.e., constant mortality rates, crop yields, and baseline GDP). The global results are shown in fig. S7

(and fig. S8 for individual crop details). For both infant mortality and crop production, the spatial pattern of aerosol physical impacts is the main driver of the total impact, at both the global and country level (insets). For GDP, the impacts are driven both by different physical impacts (magnified by the quadratic damage function) and the distribution of people (and therefore economic activity). For all three outcomes, underlying vulnerability plays a relatively small role.

Social costs of aerosol emissions are substantial relative to those of coemitted CO_2 and modify mitigation incentives

The diversity and spatial heterogeneity of these computed economic, human health, and agricultural damages that result when identical aerosols are emitted from different regions suggest that including these effects in an aggregate social cost of anthropogenic activity would introduce new geographic structure to mitigation cost-benefit analyses. To contextualize this, we normalize the constant aerosol emissions used in our perturbation experiments to coemitted CO_2 emissions to scale our experimental conditions onto more realistic scenarios. We conduct this normalization using both global-average (table S7) and region-specific (table S8) BC:CO_2, OC:CO_2, and SO_4:CO_2 ratios drawn from spatially explicit inventories (*50*) to show how the local emissions portfolio changes this calculation (fig. S15 shows the spatial and sectoral heterogeneity of these regional average ratios).

These normalized impacts provide a direct estimate of how aerosols modify the damages associated with marginal carbon dioxide emissions or the SCC (Fig. 3). We monetize impacts using average crop prices (*51*) and standard methods for estimating the value associated with premature mortality [value of statistical life (VSL); see Methods] (*52*–*54*). We show impacts per metric ton of CO_2 both in physical and monetary units to facilitate both multiattribute and single-dimensional benefit-cost analysis. When aggregating impacts across sectors, we sum up mortality and GDP impacts, but not agricultural production, because agricultural production is recorded within GDP (see Methods).

We find that, on a per metric ton of CO_2 basis, the coemissions of aerosols add $4 to $139 to the value of the CO_2-only global SCC (GSCC) ($418/t$CO_2$). These numbers grow under other assumptions about the VSL (Fig. 3), in some cases, exceeding the GSCC. The aerosol-based modification to the GSCC is highest for Indian emissions, reflecting mortality impacts that are not offset by global total increased economic output. The modification is lowest in percentage terms for Brazil ($4.44) and Indonesia ($5.65), although the values for Europe and the United States are lower if a global average VSL is used. These smaller regional impacts are due to either smaller effects in both domains (e.g., the United States) or offsetting effects (Brazil). Figure 3 shows the total impacts across GDP and mortality pathways; the corresponding table S8 shows that, across all emitting regions, these totals are dominated by the excess mortality costs.

When compared to the damages from CO_2 that accrue at the national level [i.e., the country-level SCC (CSCC) (*4*)], taking into account the effects of the localized aerosol impacts markedly alters the cost-benefit calculus for many emitting regions (Fig. 3, red

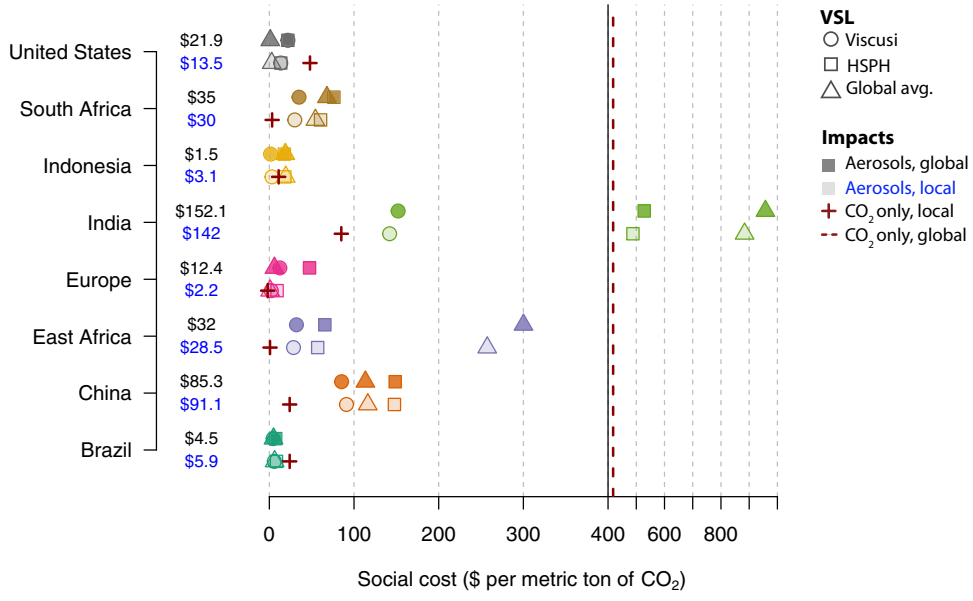

Fig. 3. The per-CO_2 normalized aerosol social costs estimated in this study. Impacts are the sum of GDP effects and infant mortality (GDP is assumed to include agricultural impacts, but a comparison of these is shown in fig. S16). Social costs are calculated here using a regionally specific aerosol-to-CO_2 emission ratio to scale the per-emission impacts derived from our experiments and three different VSL values. VSL values from Viscusi and Masterman (*52*) (circles) are derived by scaling United States Environmental Protection Agency values to other countries based on their relative gross national income and local stated preferences about willingness to pay for reduced risk of death. VSLs from the Harvard School of Public Health [squares, from Robinson *et al.* (*53*)], scale United States and Organisation for Economic Co-operation and Development member country values based on different elasticities (here, 1). Last, triangles show the social cost of aerosols using the global average VSL ($1.8 M) from Viscusi and Masterman (*52*) The dashed red line is the central value for the GSCC ($418 metric ton of CO_2) from Ricke *et al.* (*4*). Red crosses show the CO_2-only CSCC from the same source (*4*) or the portion of CO_2-related damages that accrue locally. In many cases, local aerosol social costs exceed the CSCC. Dollar values in black and blue correspond to the global and local aerosol impacts, respectively, calculated with Viscusi VSL (*52*); table S9 shows all values. CO_2-normalized local and global impacts from aerosol emissions from the eight regions are summarized in tables S8 and S7 (where impacts are scaled using a global aerosol-to-CO_2 emission ratio instead).

crosses). It more than doubles the value for China and raises it from negative to positive for Europe. India's value rises by 40%, South Africa's value rises by a factor of 10 (from \$3.3 for CO_2 alone to \$32 when localized aerosol effects are included), and Eastern Africa's value grows from less than \$1 due to CO_2-related damages to over \$30 when aerosol effects are included. These values are even higher when the local composition of emissions is taken into account. Areas with high coal and diesel emissions (China and India) have higher ratios of aerosols to CO_2 emissions and therefore a much greater fraction of social costs due to aerosol-related damages. Last, while emissions from all locations generate total global GDP benefits via cooling, we find that this is not driven by net benefits in agriculture, which we consider to be included in the total GDP benefit estimate (fig. S16). For example, most GDP gains from Indian emissions are generated locally, but crop losses total to around a 10th of that amount.

These per-unit costs enable flexible generation of emissions "scenarios" by scaling region-specific marginal impacts of aerosols coemitted with CO_2 (table S7) by actual (or projected) CO_2 emissions. Figure 4 shows how the impacts generated from each regional experiment compare to four more real-world example emissions scenarios. These include two historical scenarios where regional CO_2 emissions are set to estimated emissions from 2000 and 2019, a scenario where CO_2 emissions are set to the modeled upper limit fair-share Paris target for each region and a scenario in which higher aerosol-to-CO_2 emitting regions "clean up" their emissions ratio to the global minimum ratio and maintain year 2019 CO_2 emissions levels (see Methods and Table 1, which summarizes CO_2 emissions in each scenario). Paris fair-share targets have been designed to meet the 1.5°C warming goal by bringing all countries eventually to equal cumulative per capita CO_2 emissions, with individual pathways and timelines modified by present needs and capacity (*55*, *56*). The technology scenario can be viewed as a proxy for the technology transfer and "leapfrogging" that is built into integrated assessment model projections of future aerosol emissions in developing countries (*57*).

The impacts from these emissions scenarios are generally smaller in magnitude than the regional experiments, with China the notable exception, as prescribed aerosol emissions in the regional experiments roughly match year-2000 aerosol emissions in China. The historical real-world emissions scenarios reveal the strong aerosol-based mortality and crop production impacts, mostly damages, of the past two decades of development. They also quantify the associated substantial benefit to global GDP from historical and current aerosol cooling. The Paris fair-share scenario highlights how these targets, while obviously beneficial for climate stability, do not improve mortality and crop impacts relative to 2019 emissions, largely because the equity principles behind the fair share targets lead to the most mitigation from the United States and the European Union relative to other regions (whose emissions may even increase slightly), and the United States and the European Union per-CO_2 aerosol impacts are lower than for other regions (table S9). This indicates the potential benefits of targeted measures to reduce aerosol emissions directly to supplement reductions of aerosol coemissions with CO_2. The technology scenario, which maintains year 2019 CO_2 but reduces aerosol coemissions intensity for higher aerosol-to-CO_2 emitters, illustrates how these targeted aerosol emissions reductions could substantially improve infant mortality and crop damages. While these simulations are highly stylized and unlikely to precisely represent specific real-world scenarios, they show how the estimates of the marginal impacts of aerosols coemitted with CO_2 computed in this analysis could be used to inform policy analysis. They also again demonstrate the importance of the integrated modeling framework used here, which allows for geographically resolved and differentiated societal impacts along both air quality and climate pathways, as evidenced by the finding that global impacts of each region and outcome do not simply scale with the amount of emissions. Rather, the impacts scale with emissions differently depending on the source location and specific societal outcome.

DISCUSSION

Although warming from anthropogenic CO_2 emissions creates heterogeneous impacts around the world, these CO_2-specific damages are independent of emission location. The key conclusion of this analysis is that the dynamics of aerosol damages are entirely different: their short-term local and global impacts are strongly dependent on the location of emission, and heterogeneity in those impacts is strongly driven by the physical interactions between aerosols and the general circulation, not simply the spatial dispersion of aerosols or the simple distribution of affected human systems or their underlying vulnerabilities. Therefore, because aerosols are coemitted with CO_2, accounting for them in the social cost of emissions fundamentally changes the mitigation paradigm. The analysis presented here builds on previous work to characterize these different types of anthropogenic emissions (*10*, *15*, *22*, *58*), through use of a coupled climate-chemistry model, and extends and formalizes these ideas by creating an experimental framework and methodology to more fully assess the full impact of a diverse emissions portfolio in a physically consistent manner.

The importance of our full-system approach that jointly considers both air quality and climate pathways is illustrated in fig. S10, which shows how crop impact estimates vary when they are assessed using only AOD versus AOD, temperature, and precipitation. Considering AOD impacts alone, global damages exceed local damages for all regions; however, when changes in temperature and precipitation are also considered, local damages exceed global damages for half of the regions and two regions switch from negative to positive estimated global impacts. While the chemical transport models (and reduced complexity models) used in previous research are extremely useful for building detailed source-receptor matrices for direct pollution impacts, this spatial resolution comes at the expense of assessing aerosol climate-mediated impacts. Our results (evaluated at the roughly two degree resolution of CAM5) suggest that climate-mediated aerosol impacts are both important in magnitude and may create different and more complicated incentive structures for mitigation than implied in chemical transport model–based studies. For example, global aerosol impacts on GDP per metric ton of CO_2 emitted (a purely climate-mediated impact) vary by region of emission from around 4% (East Africa) to more than 50% (Indonesia) of the magnitude of global infant mortality impacts (a direct impact of aerosol distribution) but with the opposite sign.

By assessing the impacts of identical emissions from multiple major source regions, we are able to identify the geographic distribution of marginal damages and, consequently, of mitigation incentives for each source region, enabling mapping of cooperation incentives and optimal mitigation investments. Inclusion of impacts of coemitted aerosols and their precursors changes both the global and localized

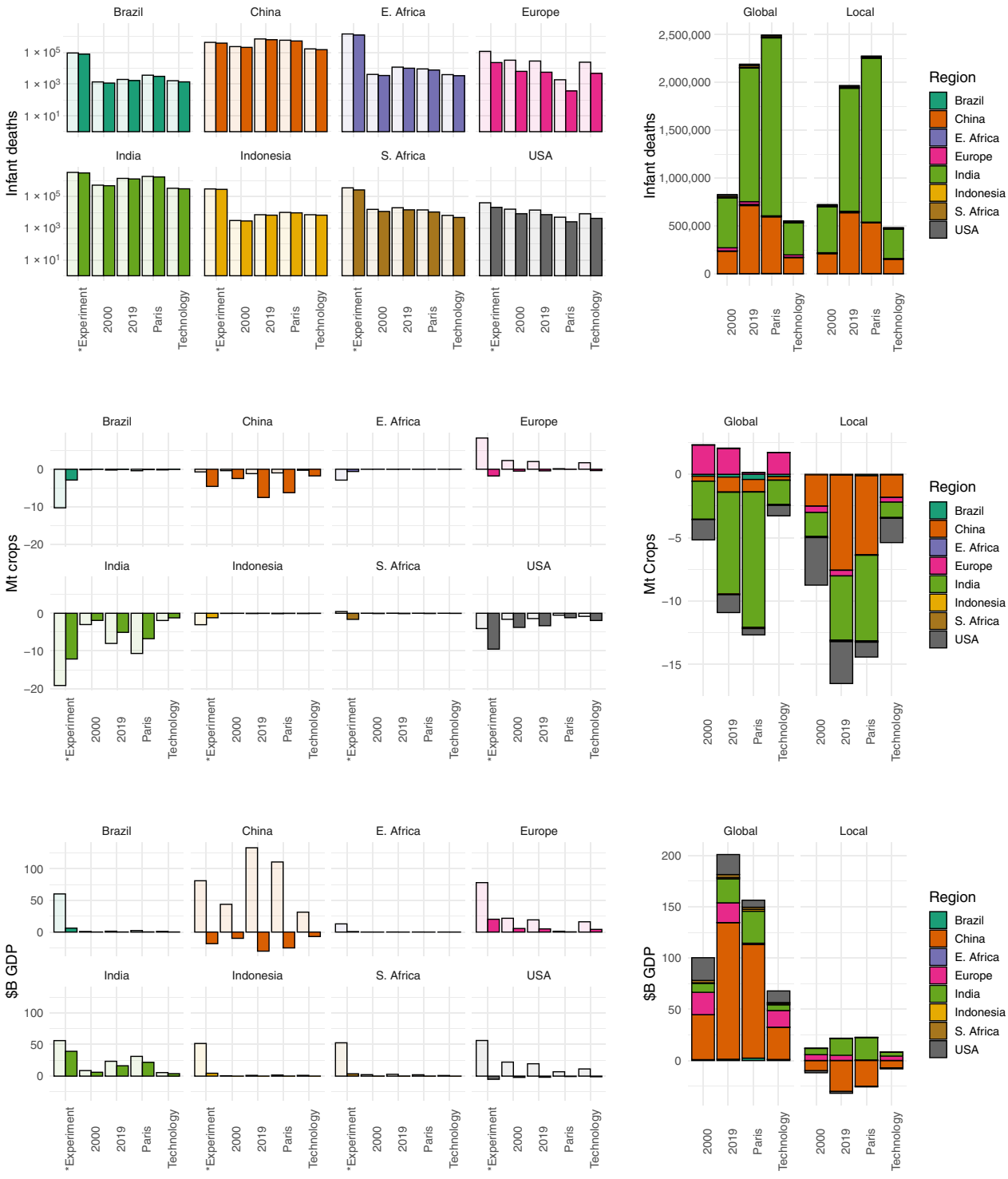

Fig. 4. Emissions scenarios and their estimated societal impacts. We map the annual impacts from our experimental conditions to a more real world context by scaling per-CO_2 aerosol impacts to different annual emissions scenarios. Left panels show how region-specific impacts presented above ("*Experiment") scale to actual year 2000 and year 2019 emissions, as well as the fair-share Paris targets ("Paris") and a scenario in which regions with higher-than-average aerosol-to-CO_2 emissions ratios (i.e., dirtier emitters) improve their emissions ratio to the global average ("Technology"). Light bars show global impacts from each emitting region, and dark bars show local impacts (corresponding data are presented in table S13). Right panels show global total impacts from these eight emitting regions added together for each scenario, as well as the portion of those impacts that accrues locally (i.e., emissions and impacts within the same region).

Table 1. Scenarios to contextualize experimental (equal-by-region) results. The first three columns show the CO_2 emissions by region for the year 2000, year 2019, and Paris fair-share scenarios. The technology scenario uses year 2019 CO_2 emissions but scales the aerosol-to-CO_2 ratio for above-average regions to the global average, as shown in the last two columns.

	Year 2000	Year 2019	Fair share	Regional ratio	Technology ratio
	Gt CO_2	Gt CO_2	Gt CO_2	Aerosol to CO_2	Scaling factor
Brazil	0.320	0.460	0.860	0.001	0.829
China	3.330	10.110	8.400	0.005	0.236
East Africa	0.020	0.070	0.050	0.003	0.336
Europe	6.120	5.410	0.360	0.001	0.843
India	0.970	2.600	3.460	0.004	0.239
Indonesia	0.260	0.610	0.860	0.001	1
South Africa	0.380	0.480	0.350	0.003	0.330
United States	5.960	5.250	1.860	0.002	0.581

costs associated with anthropogenic emissions. For the eight emitting regions, inclusion of these effects should raise marginal willingness to pay for mitigation of emissions in global and purely self-serving ("localized") terms. Perhaps unexpectedly, even when using nonlinear damage functions that have the potential for positive impacts (benefits) to aerosol emissions, we find that local impacts are always negative. This is a critical note, because simultaneous mitigation of shorter-lived pollutants and CO_2 would be expected to amplify local warming in the short run by removing the aerosol-driven cooling (e.g., Fig. 1) that currently masks a portion of longer-run greenhouse gas–driven warming.

At the regional scale, these analyses suggest that inclusion of coemitted aerosol impacts may change the nature of cooperation incentives as well. It has been noted that Arctic nations would benefit from formation of mitigation "clubs" outside the international climate change framework (*59*). When we aggregate our estimated impacts from the eight test regions and consider each as both sources of emissions and receptors of impacts (fig. S9 and tables S10 to S12), we see that the receptor regions' interests lie disproportionately across subgroups of source regions and thus that the potential for mitigation clubs also arises here. The regional pairs of Eastern Africa and India and India and China share strong connections for infant mortality and crop impacts that might incentivize additional mitigation, even for these emerging economies. Europe, the United States, and China exert strong temperature-driven GDP impacts around the world that meaningfully change the financial value of mitigation for each region, whether considering global or localized impacts. Although these 8 × 8 matrices are only a subset of source/receptor relationships, this framework provides a roadmap for the type of analyses that should eventually underlie valuation of the full suite of emissions from human activity and how their downstream effects are "traded." Impacts of each source region globally, on specific receptor regions, and locally are different for each type of societal impact. An understanding of a full suite of impacts and relationships would thus allow each country to proceed with mitigation decisions according to their own valuations of damages and partnerships across the globe.

This analysis has several limitations that suggest that specific impact numbers should be interpreted cautiously. We start from a framework of identical emissions from each source region to appropriately disentangle the effect of the physical Earth system—how it processes and disperses aerosols from different locations—from the underlying heterogeneous distributions of populations and land uses at the Earth's surface. Although we subsequently normalize results to make them more easily translatable to present conditions, this analysis underscores the importance for future observationally constrained emissions inventories to both probe potential shortcomings of the linearities assumed here and to more finely capture regional variations in emissions (this is especially important in biomass-dependent economies where inventories are known to be much less accurate) (*60*–*62*).

Our experimental design is motivated by the fact that social cost calculations, emissions accounting, and many regulatory limits use the mass of pollutant emissions as the relevant unit and that comparability across emitting regions is of great interest in international policy discussions. We, therefore, choose to equalize emissions amount across the regions in our simulations rather than atmospheric concentration or emission intensity, which are less straightforwardly translatable in these policy contexts. This could potentially introduce effects because of the differing spatial extents of the regions over which the emissions are imposed, primarily by amplifying air quality impacts in regions with a smaller spatial extent (i.e., where the emissions are more concentrated). To some extent, this reflects actual increased risks from emissions in confined regions where industrial activity is necessarily spatially concentrated and likely to be colocated with population centers (in all cases, emissions are distributed within country according to year 2000 realistic emissions distributions). However, smaller regions do not systematically exhibit stronger air quality effects or associated societal impacts in our results (e.g., Fig. 2), suggesting that this effect does not dominate.

Certain aspects of aerosols' climate effects can also be sensitive to the background aerosol concentrations onto which the additional perturbation is added. In particular, there is evidence that adding aerosol to a relatively pristine atmosphere results in (in some cases, two times) larger marginal radiative and cloud effects than adding aerosol to a relatively dirty atmosphere (*63*, *64*), but confidence in this effect is low (*65*, *66*). Constructing equal emissions perturbation experiments such as ours will necessarily require making certain decisions about the background climate onto which emissions are added. The aerosol background onto which we add our equal emissions perturbation is not pristine (year 2000 biomass burning aerosols and natural background dust and sea salt aerosols are present in

both the control and perturbation experiments) nor is it as polluted as the present-day atmosphere (other anthropogenic aerosol are set at 1850 levels in the control). Hence, the marginal physical system effects calculated from our simulations could be viewed as a slight overestimate of the effects of future marginal changes in aerosol emissions, if background atmospheric aerosols increase, or as a slight underestimate, if they decline—both of which are contemplated in future emissions scenarios (*67*).

The damage functions we use are derived from empirical statistical studies of annual outcomes. They thus capture adaptations to short-run changes in physical states (such as a farmer irrigating in response to a series of hot days) but do not capture long-run adaptations (such as a farmer installing irrigation in response to a warmer climate). Hence, long-run adaptation may cause realized outcomes to differ from simulated responses. We also note that, in addition to spatial colocation of physical changes and human systems, the temporal dimension also affects calculations of societal damages based on these damage functions. Crops are sensitive to environmental changes within their location-specific growing season. Figure S12 shows the local climatology from the control scenario for each source region along with perturbations to that climatology created by emissions from each source region. For example, Europe's local temperature impacts are strongly concentrated in the summer growing season months, whereas South Africa's are year-round; Eastern Africa's precipitation effects are primarily in the second rainy season, whereas Indonesia's are year-round. Similarly, although we calculate average annual effects on infant mortality, given that we find strong seasonal variation in $PM_{2.5}$ concentrations driven by transport and deposition mode timing, we would expect that the variation in total $PM_{2.5}$ burden, as well as individual BC, OC, and sulfate burdens (fig. S13), would vary at subannual scales. Better understanding of the fidelity of the seasonal behavior of both physical models and damage functions will thus be an important component of improving damage estimates going forward.

The results should also be interpreted in the context of the subset and mix of coemissions applied here. The potential attractiveness of CO_2 + aerosol mitigation would be expected to change if new technologies (e.g., diesel truck filters) altered the ratio of aerosol to CO_2 emissions. These technologies can also preferentially mitigate specific aerosol species over others (e.g., SO_2 scrubbers on coal-fired power plants) to achieve optimal societal outcomes. We choose to impose a mixture of aerosol emissions (sulfate, BC, and OC) that captures the aerosol mix present in a modern industrial economy (i.e., China; see Methods), because many industrial processes coemit these species, and their trajectories vary in concert across future emission scenarios (*57*, *68*, *69*). However, because we impose an aerosol suite rather than individual aerosol species, the effects we quantify should be construed as a proxy for the effects of economy-wide aerosol emission changes rather than as the effects of implementing any specific technology. Variations in individual aerosol species may produce different and potentially nonadditive physical system effects compared to the aggregate effects imposed here (*70*), and future work will explore this. In addition, in particular regions, other aerosol precursors such as nitrates and volatile organic compounds can contribute substantially to surface $PM_{2.5}$ levels, although the source apportionment and fidelity of emissions inventories for these compounds remain challenging (*37*). Hence, the infant mortality estimates given here likely constitute an underestimate of the true damages associated with all non-GHG coemissions. This further underscores the importance of spatially, temporally, and sectorally resolved multispecies inventories to anchor benefit-cost analyses of all human activities that generate emissions.

Last, our analyses here include only a small subset of aerosol-related impact pathways, selected because they involve responses that occur over shorter (and, therefore, separable) time scales, have large welfare implications, and for which response functions are well established. However, aerosols are expected to exhibit impacts through other pathways—for example, $PM_{2.5}$ has been shown to have impacts on adult morbidity and mortality, cognitive performance, and productivity (*44*, *71*, *72*); aerosol-driven radiation effects would be expected to affect forests and native habitats in addition to crops (*73*–*75*); and changes in temperature and precipitation have been linked to other important social impacts besides economic output (*76*, *77*)—that are not included here. In addition, other coemitted pollutants—including heavy metals, high-GWP gases, and especially ozone precursors such as NOx, methane, and other volatile organic compounds—are known to affect human health, plant health, and climate. NOx itself is a main precursor to nitrate aerosols, and the ability of future models to more fully include nitrogen and other secondary organic aerosol dynamics into this framework will be critical. Our analyses do not replicate the highest pollution levels currently observed globally—this is more an "average modern" idealization—and thus, we do not capture dynamics specific to the highest pollution levels including likely smaller marginal responses to each additional unit of $PM_{2.5}$. Future empirical work estimating heterogeneous climate and social effects of regional aerosol emissions, such as those from volcanic eruptions or fires, and at higher baseline pollution levels, could provide both valuable evaluation of our findings and improved exposure-response functions to incorporate into this framework. This analysis thus represents a starting point for consideration of the full suite of human emissions and their impact pathways.

METHODS

Climate model perturbation experiments

This study uses nine 100-year, repeating annual cycle simulations conducted in the NCAR CAM5, run with the modal aerosol module with three log-normal modes (MAM3) and coupled to a mixed-layer ocean. Full details on the simulation setup may be found in Persad and Caldeira (*8*).

We conduct a control simulation using year 2000 climate conditions, including year 2000 atmospheric concentrations of carbon dioxide (367 parts per million) and other greenhouse gases, with nonbiomass burning anthropogenic aerosols (BC, SO_2, and OC) fixed at 1850 values. We then conduct eight regional perturbation experiments in which a total annual emission of 22.4 Tg of SO_2, 1.61 Tg of BC, and 4.03 Tg of OC emissions—equivalent to China's year 2000 emissions in CAM5's baseline emissions inventory (*78*)—is added to one of the eight source regions, defined according to the Intergovernmental Panel on Climate Change's regional definitions. We opt to focus on this suite of short-lived pollutants because of their dominant role in both climate and air quality impacts. We exclude secondary pollutants, such as tropospheric ozone and nitrate-based secondary aerosol, for which computationally prohibitive interactive gas-phase chemistry would be required and for which geographic source apportionment is not straightforward. This fixed emissions burden is distributed within the given source

region according to that region's year 2000 values (i.e., according with the realistic within-region distribution of emissions sources), scaled equally at each grid point and time step to produce the desired total addition. Within-region emissions distributions are shown in fig. S14. The difference between each regional perturbation simulation and the control simulation thereby captures the climate response to the addition of an identical total annual aerosol emission located in a given region.

The eight regions are selected to sample a range of past, present, and projected future major source regions of aerosol emissions. Europe and the United States dominated nonbiomass burning aerosol emissions through the second half of the 20th century; China and India are currently the largest source regions of aerosol emissions; and Indonesia, East Africa, South Africa, and Brazil are all regions where aerosol emissions are projected to grow substantially over the early 21st century across the Representative Concentration Pathway and Shared Socioeconomic Pathway scenarios (*68*, *78*, *79*). The selection of regions, which are located in a range of climatological environments, also allows us to test the sensitivity of the responses to dominant atmospheric and climate processes present in the Northern and Southern Hemisphere mid-latitudes, tropical regions, monsoonal regimes, and upwind and downwind of the major ocean basins.

Our use of a fully coupled earth system model allows us to assess combined climate and air quality impacts of aerosols from the different regions in a fully consistent and physically integrated way. Given that many societal damage functions indicate that societal outcomes respond nonlinearly to combined climate and air quality pressures (represented most clearly in this study in crop yields (*39*)), the simultaneous, internally consistent simulation of these effects that our methodology provides is particularly valuable. The CAM5 model with MAM3 has been shown to produce atmospheric burdens of sulfate, OC and BC that align strongly (difference < 10%) with atmospheric models containing more complex atmospheric chemistry (*80*). The same holds for radiative forcing from historical aerosol emissions (*81*). When run with historical emissions, the model captures observed geographic and temporal patterns of aerosols concentrations. It produces low-biased AOD, particularly over East and South Asia, but this may be partially the result of uncertainties in historical emissions inventories, which our equal-emissions simulations will not be subject to (*80*). The fully coupled CESM model has demonstrated skill in simulating historical temperature and precipitation at both the global and regional scale, consistently performing among the top 10 or top half of the Fifth Coupled Model Intercomparison Project (CMIP5) models for a range of climate metrics (*82*).

The model simulations are constructed as equilibrium or "time-slice" simulations to allow quantification of the response to the imposed aerosol perturbation with a robust signal to noise ratio [see e.g., (*83*, *84*)]. Output from the model is monthly, nominal 2° (144 × 96) grids, in netcdf format. The first 40 years of the time-slice simulations are excluded to allow the model to stabilize from initial conditions (determined by when trends in sea surface temperature and top-of-atmosphere energy imbalance become negligible), and analysis is conducted on the past 60 years (720 months) of data as the steady-state response. Each year can be treated as an "ensemble member" (so, parameters for this period are calculated for $n = 60$), because of the primarily subannual effects of aerosols and minimal autocorrelation between years. From experiment and control condition runs, we extract the following variables: surface BC, OC, and sulfate mixing ratios, surface temperature, surface pressure, precipitation, and column AOD. We add surface BC, OC, and SO_4 and convert to concentration using local temperature and pressure. For each variable, we then calculate mean changes between each source region and the control condition (e.g., Fig. 1), and we aggregate over both the source region and the globe to compare local versus global changes (e.g., fig. S4).

Damage functions and their application

From perturbation experiments, we calculate spatially explicit changes in four summary physical responses ΔPM_{cs}, ΔAOD_{cs}, ΔT_{cs}, and ΔP_{cs} where for each, c is the receptor cell and s is the source region where the aerosols were emitted. Values are aggregated to either annual average changes (infant mortality and GDP) or crop-growing-season averages (corn, wheat, rice, and soybean) in each physical parameter, relative to the control runs.

To connect these physical changes to human-related damages, we then use existing empirically estimated damage functions that relate changes in these parameters to changes in infant mortality, changes in production from major crops, and changes in economic output. We use published damage functions from studies that use panel data (repeated observations of many locations over time) and fixed-effects regression models to isolate variation in the exposure of interest (e.g., temperature or $PM_{2.5}$) from other time-invariant and time-varying factors that could be correlated with both this exposure and the outcome of interest.

Changes in infant mortality

To understand impacts on human life, we relate ΔPM_{cs} to changes in infant mortality. Impacts are calculated on the basis of the exposure-response function in Heft-Neal *et al.* (*38*), who in a study of nearly a million African births find that the infant mortality rate (IMR) increases linearly with $PM_{2.5}$ exposures, with a 0.9% increase in infant mortality per 1 $\mu g/m^3$ increase in $PM_{2.5}$ (table S2). While this response was estimated in the African context, other work has suggested strong similarity in the relative response of IMR to $PM_{p2.5}$ across both the developed and developing world from studies that use similar quasi-experimental methodologies (*85*–*87*). That is, while the total number of infant deaths that occur as a result of a unit increase in PM exposure declines substantially at lower baseline IMR, the proportional impact—i.e., the percent increase in IMR per unit increase in PM—is, if anything, empirically smaller in lower-income higher-mortality regions (fig. S11), perhaps because there are more competing risks for infant death in lower-income regions. Thus, assuming a constant proportional increase based on the African estimate is likely a lower bound on the proportional increase in much of the rest of the world. Total additional excess infant deaths in each receptor country are then calculated as

$$\Delta IM_{cs} = \Delta PM_{cs} * \beta^{IMR} * IMR_c * I_c \quad (1)$$

where ΔPM_{cs} is the change in infant population–weighted surface particulate matter, $\beta^{IMR} = 0.009$ is the percentage increase in IMR per unit increase in particulate matter (see table S2), IMR_c is the baseline infant mortality rate in each country (*88*), and I_c is the estimated infant population in each country (*89*) [we approximate the under-1 population as one-fifth of the under-5 population provided in (*89*)]. ΔIM_{cs} then gives total excess infant mortality in each country

c in a single average year due to emissions in source region *s*, relative to a no-aerosol scenario.

Parameter uncertainty in infant deaths for each scenario is calculated on the basis of the SEs of the empirical estimate in (*38*) (table S2); uncertainty due to internal climate variability is calculated from variation in $\Delta PM_{2.5}$ across the 60 ensemble members. While many estimates of this impact coefficient (β^{IMR}) exist in the literature, we use the coefficient from (*38*) because it draws on nearly a million births that spans one of our test regions (Eastern Africa, for which there are no other estimates) and is not statistically different from estimates drawn from other study regions (e.g., the United States, Europe, and China) (fig. S11). Moreover, linearity in the response over the relevant range of $PM_{2.5}$ concentrations is consistent with other available mortality response functions estimated for different age groups (*90*–*92*).

Changes in crop production

To calculate changes in crop production, we use estimates from Proctor *et al.* (*39*), who used variations in AOD created by large volcanic eruptions to estimate the impacts of aerosol-driven radiation changes on crop yields while also accounting for changes in temperature and precipitation also driven by the atmospheric aerosol burden. We calculate change in total production of each of four main staple crops (maize, wheat, rice, and soybean) as

$$\Delta \mathrm{PROD}_{jcs} = [\Delta Y_{\mathrm{jcs}} * Y_{jc}] * A_{jc} \quad (2)$$

where Y_{jc} is the baseline yield of each crop *j* in country *c* and A_{jc} is the baseline area, where for both we use the estimated 2000 area and yields from (*93*). The percentage change in yield ΔY_{jcs} is calculated by applying $\Delta \mathrm{AOD}_{cs}$, ΔT_{cs}, and ΔP_{cs} to the response functions estimated in Proctor *et al.* (*39*) and is done as follows

$$\Delta Y_{jcs} = \Delta f(\mathrm{AOD}_{jcs}) + \Delta f(T_{jcs}) + \Delta f(P_{jcs}) \quad (3)$$

where we apply model coefficients to changes in temperature, precipitation, and AOD (table S3) over crop-specific growing seasons (*94*) and areas in each country to calculate national-level yield changes. Specifically, we calculate changes in yield at the pixel-growing season resolution and then average over space (cropped-area weighted average of pixels within a country) and time (60 years) to get a single estimate of ΔY_{jcs} for each crop, country and source region.

Uncertainty in the crop response from imperfectly estimated empirical model parameters is calculated as in Proctor *et al.* (*39*). Uncertainty in the crop response from imperfectly estimated changes in the climate variables is calculated, for each crop, country, and source region as the SE of Y_{jcst} over years, *t*.

Changes in economic output

To calculate changes in macroeconomic output, we use response functions from Burke *et al.* (*40*), who find that per capita national economic growth varies strongly and nonlinearly with annual average temperature. We calculate the change in total economic output in each country *c* due to the change in temperature from aerosols from source region *s* as

$$\Delta \mathrm{GDP}_{cs} = [f(T_c + \Delta T_{cs}) - f(T_c)] * \mathrm{GDPpc}_c * \mathrm{pop}_c \quad (4)$$

where GDPpc_c and pop_c are the baseline (2010) per capita GDP and population in country *c* and *f*() is the function from Burke *et al.* (*40*) that estimates the percentage change in per capita GDP in a given year from a change in temperature: $f() = \beta_1 T_{ct} + \beta_2 T_{ct}^2$, where T_{ct} is the annually averaged temperature in country *c* in year *t*. Coefficients and standard errors for β_1 and β_1 are given in table S4. $\Delta \mathrm{GDP}_{cs}$ then gives the total change in GDP in country *c* over 1 year due to aerosol emissions from source region *s*.

As for infant mortality and crop production, we estimate SEs on the basis of the statistical model parameter uncertainty and due to the internal variability of the climate system (e.g., error bars shown in fig. S4).

Partitioning aerosol impacts

A key question is the extent to which aerosol impacts on human systems are driven by changes in the physical system versus the distribution of underlying human systems and/or their baseline vulnerabilities. To assess this, we compare the results from our main experiments with impacts estimated from three counterfactual scenarios:

1) Globally homogeneous physical changes: In this scenario, we use the global-mean change in all parameters induced by aerosols instead of the locally resolved changes.

2) Globally homogeneous distribution of human systems: In this scenario, we spread human systems (infant populations, crop area, and human populations) equally over all land areas.

3) Globally homogeneous vulnerability: In this scenario, we assume all human systems (infant mortality, crop yields, and per capita GDP) are held at the global average as opposed to their local values.

We estimate impacts from each emissions region for these three additional scenarios for each of the three impact pathways and compare the results in figs. S7 and S8. At the global level (fig. S7, left), we find that the physical system changes (i.e., the geographic heterogeneity of aerosol interactions with the general circulation from different regions) are the main contributor to both excess infant mortality and crop production changes; the green bars or the estimates of impacts from a counterfactual homogeneous physical system response are most different from the actual experimental conditions, shown by the gray bars. For macroeconomic (GDP) impacts, the combination of physical system impacts and underlying population distributions (the generators of economic activity) both exert strong influences, but across scenarios, the physical impacts are consistently the major drivers, while population distribution importance varies across emission regions.

To more concretely understand the relative importance of these factors, we conduct a simple analysis at the country level from the above simulations (fig. S7, right). We use a regression model to understand how within-country estimates change as a function of each of the factors, using the actual experiments across source regions and the counterfactual scenarios above. These findings suggest that, on average, the physical system is the primary main driver of impacts at the national scale and is not dominated by (e.g.) the national-level vulnerabilities or population distributions on average. The macroeconomic impacts are much more heterogeneous, likely due to the nonlinearity in the damage function. Aerosol-driven cooling improves economic output in countries whose climatological temperature is above the economic optimum and damages output in those below.

Contextualizing aerosol impacts

In addition to the absolute damages (table S5), we report the damages normalized by the total aerosol emissions perturbation (28.04 Tg of

combined BC, OC, and SO_2 for each scenario; table S6). We then additionally normalize to CO_2 emissions in two ways, as described below.

While aerosols and their precursors are emitted in many combustion processes, the relative production of these compounds (compared to CO_2) varies by technology, feedstock, and combustion conditions, and this is manifest in regional- and sectoral-scale differences in aerosol-to-GHG emissions ratios. (*50*) We scale the equal-aerosol-emission results described above by converting from a per-Tg aerosol basis to a per-CO_2 basis using either a global average aerosol-to-CO_2 emissions ratio (table S7) or a region-specific ratio (table S8). Both ratios [i.e., (BC + OC + SO_2)/CO_2] are drawn from the Emission Database for Global Atmospheric Research global emissions inventory (*50*). These values are then locally specific estimates of the impact of the concomitant aerosol emissions coproduced with a metric ton of CO_2 emissions from that region. We include all CO_2 emissions, including short-cycle CO_2, to calculate this ratio.

We use these per-unit regional results to create a set of four global scenarios (Table 1) by scaling unit-level aerosol impacts per CO_2 emission (table S7) to different regional levels of CO_2 emissions. Using data from the Global Carbon Project (GCP) (*95*), we first scale to historical 2000 and 2019 CO_2 emissions from each region to show the evolution of regional contributions. (We note that the GCP inventory differs slightly from the CAM5 baseline inventory used in our experimental simulations.) We then additionally coarsely model the impact of "fair share" 2030 Paris targets taken from the Climate Action Tracker (*55*). The fair share method seeks to balance mitigation effort equitably across the globe. In this approach, countries' cumulative emissions per capita eventually converge for equity, but the pathway by which each arrives at that value varies according to their capability and needs (*55*, *56*). Here, we use the upper limit of the fair-share range compatible with the global +1.5C target; for Eastern Africa, we follow the modeled pathways for Kenya and Ethiopia, which put 2030 emissions at approximately 77% of 2019 level emissions. Last, we simulate global improvements in the aerosol-to-CO_2 ratio by reducing regional aerosol-to-CO_2 ratios to the lowest regional average value (Table 1; Indonesia, Europe, and Brazil have the lowest ratios). This scaling is an approximation of technology transfer to regions (and in sectors) with "dirtier" production.

Social cost of emission calculations

Policy analysts face a choice between accounting for benefits and damages across different units (e.g., premature deaths, metric tons of wheat, and dollars of GDP) using multiattribute methods or converting all benefits and damages to a common unit (typically currency) for a single-dimensional benefit-cost analysis. To facilitate the latter, we convert infant mortality and crop production impacts to U.S. dollar values using standard methodologies (these are both presented in tables S7 and S8). We note that welfare impacts may differ considerably from monetary impacts (e.g., a lost metric ton of wheat production likely reduces the welfare of a subsistence farmer more than a large-scale producer).

To convert crop production changes to monetary values, we use an average crop price (across the four crops) of $300/metric ton, with fig. S16 showing a comparison between low and high values of $100/metric ton to $400/metric ton. We similarly convert deaths to monetary values using value of statistical life estimates from the literature (*52*–*54*). The main values presented in tables S7 and S8 use Viscusi and Masterman (*52*) local values. However, we present social cost estimates based on an alternative region-specific VSL (*53*) and using the global average VSL ($1.8 million) from Viscusi and Masterman (*52*). This global average is lower than, for example, the value used by the U.S. Environmental Protection Agency ($9.1 million) (*54*), but numerous studies have shown a wide divergence in values across countries and different weightings for infants versus other age cohorts (*52*, *54*, *96*). Per-emission damages are multiplied by these values to estimate the aerosol-related changes to the SCC (both GSCC and CSCC). These parameters could take on a wide range of values, but as the goal here is to demonstrate how inclusion of coemitted aerosols changes the social cost of a CO_2 emission, we have used these low-to-moderate values for conservative estimates.

We use Ricke *et al.* (*4*) as a baseline value for both the GSCC and the CSCC. The GSCC represents the global total damages estimated to accrue from a marginal future metric ton of CO_2 emissions, and the CSCC represents the portion of those damages accruing to each country (irrespective of location of emission). Although Ricke *et al.* (*4*) represents a higher GSCC than values currently used in policy (and some others suggested in studies), it is ideal for comparison because it provides a self-consistent estimate of both country-level and global-level SCCs. We extend this methodology here by comparing the social costs (via infant mortality, crop production, and economic output) due to aerosol emissions that are coproduced with CO_2 to the CO_2-only values. Because aerosol atmospheric lifetimes are much shorter than CO_2 (days to months versus decades to centuries), we assume a separability of time scales and calculate aerosol-related damages on an annual basis, without any discounting.

Significance statement

Carbon dioxide affects the Earth's climate independent of where on the planet it is released into the atmosphere. However, most CO_2 is coemitted with other pollutants such as aerosols and aerosol precursors that are not similarly long lived or well mixed in the atmosphere. Here, we show that emitting the same aerosols from different locations produces very different physical climate responses, which in turn create divergent impacts on human health, agricultural production, and economic output. Consideration of these coemitted aerosols thus markedly changes the SCC, with important geographic variations and linkages.

SUPPLEMENTARY MATERIALS

Supplementary material for this article is available at https://science.org/doi/10.1126/sciadv.abn7307

REFERENCES AND NOTES

1. R. S. Tol, The economic effects of climate change. *J. Econ. Perspect.* **23**, 29–51 (2009).
2. W. Pizer, M. Adler, J. Aldy, D. Anthoff, M. Cropper, K. Gillingham, M. Greenstone, B. Murray, R. Newell, R. Richels, A. Rowell, S. Waldhoff, J. Wiener, Using and improving the social cost of carbon. *Science* **346**, 1189–1190 (2014).
3. W. Nordhaus, Estimates of the social cost of carbon: Concepts and results from the DICE-2013R model and alternative approaches. *J. Assoc. Environ. Resour. Econ.* **1**, 273–312 (2014).
4. K. Ricke, L. Drouet, K. Caldeira, M. Tavoni, Country-level social cost of carbon. *Nat. Clim. Chang.* **8**, 895–900 (2018).
5. S. Hsiang, R. Kopp, A. Jina, J. Rising, M. Delgado, S. Mohan, D. J. Rasmussen, R. Muir-Wood, P. Wilson, M. Oppenheimer, K. Larsen, T. Houser, Estimating economic damage from climate change in the United States. *Science* **356**, 1362–1369 (2017).
6. D. Shindell, G. Faluvegi, Climate response to regional radiative forcing during the twentieth century. *Nat. Geosci.* **2**, 294–300 (2009).
7. D. T. Shindell, Inhomogeneous forcing and transient climate sensitivity. *Nat. Clim. Chang.* **4**, 274–277 (2014).

8. G. G. Persad, K. Caldeira, Divergent global-scale temperature effects from identical aerosols emitted in different regions. *Nat. Commun.* **9**, 3289 (2018).
9. D. Shindell, J. F. Lamarque, N. Unger, D. Koch, G. Faluvegi, S. Bauer, M. Ammann, J. Cofala, H. Teich, Climate forcing and air quality change due to regional emissions reductions by economic sector. *Atmos. Chem. Phys.* **8**, 7101–7113 (2008).
10. J. S. Wallack, V. Ramanathan, The other climate changers: Why black carbon and ozone also matter. *Foreign Aff.* **5**, 105–113 (2009).
11. UNEP, "Integrated assessment of black carbon and tropospheric ozone: Summary for decision makers" (Technical Report, United Nations Environment Programme and World Meteorological Organization, 2011).
12. J. Burney, V. Ramanathan, Recent climate and air pollution impacts on indian agriculture. *Proc. Natl. Acad. Sci. U.S.A.* **111**, 16319–16324 (2014).
13. M. Ikefuji, J. R. Magnus, H. Sakamoto, The effect of health benefits on climate change mitigation policies. *Clim. Change* **126**, 229–243 (2014).
14. N. Scovronick, D. Anthoff, F. Dennig, F. Errickson, M. Ferranna, W. Peng, D. Spears, F. Wagner, M. Budolfson, The importance of health co-benefits under different climate policy cooperation frameworks. *Environ. Res. Lett.* **16**, 055027 (2021).
15. K. R. Smith, M. Jerrett, H. R. Anderson, R. T. Burnett, V. Stone, R. Derwent, R. W. Atkinson, A. Cohen, S. B. Shonkoff, D. Krewski, C. A. Pope III, M. J. Thun, G. Thurston, Public health benefits of strategies to reduce greenhouse-gas emissions: Health implications of short-lived greenhouse pollutants. *Lancet* **374**, 2091–2103 (2009).
16. S. C. Anenberg, J. Schwartz, D. Shindell, M. Amann, G. Faluvegi, Z. Klimont, G. Janssens-Maenhout, L. Pozzoli, R. van Dingenen, E. Vignati, L. Emberson, N. Z. Muller, J. J. West, M. Williams, V. Demkine, W. K. Hicks, J. Kuylenstierna, F. Raes, V. Ramanathan, Global air quality and health co-benefits of mitigating near-term climate change through methane and black carbon emission controls. *Environ. Health Perspect.* **120**, 831–839 (2012).
17. J. J. West, S. J. Smith, R. A. Silva, V. Naik, Y. Zhang, Z. Adelman, M. M. Fry, S. Anenberg, L. W. Horowitz, J. F. Lamarque, Co-benefits of mitigating global greenhouse gas emissions for future air quality and human health. *Nat. Clim. Chang.* **3**, 885–889 (2013).
18. K. Tibrewal, C. Venkataraman, Climate co-benefits of air quality and clean energy policy in India. *Nat. Sustain.*, 1–9 (2020).
19. J. M. Balbus, J. B. Greenblatt, R. Chari, D. Millstein, K. L. Ebi, A wedge-based approach to estimating health co-benefits of climate change mitigation activities in the United States. *Clim. Change* **127**, 199–210 (2014).
20. J. A. Burney, The downstream air pollution impacts of the transition from coal to natural gas in the United States. *Nat. Sustain.* **3**, 152–160 (2020).
21. C. T. Driscoll, J. J. Buonocore, J. I. Levy, K. F. Lambert, D. Burtraw, S. B. Reid, H. Fakhraei, J. Schwartz, Us power plant carbon standards and clean air and health co-benefits. *Nat. Clim. Chang.* **5**, 535–540 (2015).
22. D. T. Shindell, The social cost of atmospheric release. *Clim. Change* **130**, 313–326 (2015).
23. S. Rao, Z. Klimont, J. Leitao, K. Riahi, R. van Dingenen, L. A. Reis, K. Calvin, F. Dentener, L. Drouet, S. Fujimori, M. Harmsen, G. Luderer, C. Heyes, J. Strefler, M. Tavoni, D. P. van Vuuren, A multi-model assessment of the co-benefits of climate mitigation for global air quality. *Environ. Res. Lett.* **11**, 124013 (2016).
24. A. Markandya, J. Sampedro, S. J. Smith, R. van Dingenen, C. Pizarro-Irizar, I. Arto, M. González-Eguino, Health co-benefits from air pollution and mitigation costs of the paris agreement: A modelling study. *Lancet Planet. Health* **2**, e126–e133 (2018).
25. N. Scovronick, M. Budolfson, F. Dennig, F. Errickson, M. Fleurbaey, W. Peng, R. H. Socolow, D. Spears, F. Wagner, The impact of human health co-benefits on evaluations of global climate policy. *Nat. Commun.* **10**, 2095 (2019).
26. P. Tschofen, I. L. Azevedo, N. Z. Muller, Fine particulate matter damages and value added in the U.S. economy. *Proc. Natl. Acad. Sci. U.S.A.* **116**, 19857–19862 (2019).
27. D. Shindell, G. Faluvegi, M. Walsh, S. C. Anenberg, R. van Dingenen, N. Z. Muller, J. Austin, D. Koch, G. Milly, Climate, health, agricultural and economic impacts of tighter vehicle-emission standards. *Nat. Clim. Chang.* **1**, 59 (2011).
28. D. Shindell, J. C. I. Kuylenstierna, E. Vignati, R. van Dingenen, M. Amann, Z. Klimont, S. C. Anenberg, N. Muller, G. Janssens-Maenhout, F. Raes, J. Schwartz, G. Faluvegi, L. Pozzoli, K. Kupiainen, L. Höglund-Isaksson, L. Emberson, D. Streets, V. Ramanathan, K. Hicks, N. T. K. Oanh, G. Milly, M. Williams, V. Demkine, D. Fowler, Simultaneously mitigating near-term climate change and improving human health and food security. *Science* **335**, 183–189 (2012).
29. D. Shindell, G. Faluvegi, K. Seltzer, C. Shindell, Quantified, localized health benefits of accelerated carbon dioxide emissions reductions. *Nat. Clim. Chang.* **8**, 291–295 (2018).
30. J. Lelieveld, K. Klingmüller, A. Pozzer, R. T. Burnett, A. Haines, V. Ramanathan, Effects of fossil fuel and total anthropogenic emission removal on public health and climate. *Proc. Natl. Acad. Sci.* **116**, 7192–7197 (2019).
31. D. T. Shindell, A. Voulgarakis, G. Faluvegi, G. Milly, Precipitation response to regional radiative forcing. *Atmos. Chem. Phys.* **12**, 6969–6982 (2012).
32. H. Wang, S.-P. Xie, Q. Liu, Comparison of climate response to anthropogenic aerosol versus greenhouse gas forcing: Distinct patterns. *J. Climate* **29**, 5175–5188 (2016).
33. B. Aamaas, T. K. Berntsen, J. S. Fuglestvedt, K. P. Shine, W. J. Collins, Regional temperature change potentials for short-lived climate forcers based on radiative forcing from multiple models. *Atmos. Chem. Phys.* **17**, 10795–10809 (2017).
34. D. M. Westervelt, A. J. Conley, A. M. Fiore, J. F. Lamarque, D. T. Shindell, M. Previdi, N. R. Mascioli, G. Faluvegi, G. Correa, L. W. Horowitz, Connecting regional aerosol emissions reductions to local and remote precipitation responses. *Atmos. Chem. Phys.* **18**, 12461–12475 (2018).
35. G. Myhre, D. Shindell, F.-M. Breon, W. Collins, J. Fuglestvedt, J. Huang, D. Koch, J.-F. Lamarque, D. Lee, B. Mendoza, T. Nakajima, A. Robock, G. Stephens, T. Takemura, H. Zhang, Anthropogenic and Natural Radiative Forcing in *Climate Change 2013: The Physical Science Basis. Contribution of Working Group I to the Fifth Assessment Report of the Intergovernmental Panel on Climate Change*, T. F. Stocker, D. Qin, G.-K. Plattner, M. Tignor, S. Allen, J. Boschung, A. Nauels, Y. Xia, V. Bex, P. Midgley, eds. (Cambridge University Press, Cambridge, United Kingdom and New York, NY, USA, 2013), pp. 659–740.
36. G. Snider, C. L. Weagle, R. V. Martin, A. van Donkelaar, K. Conrad, D. Cunningham, C. Gordon, M. Zwicker, C. Akoshile, P. Artaxo, N. X. Anh, J. Brook, J. Dong, R. M. Garland, R. Greenwald, D. Griffith, K. He, B. N. Holben, R. Kahn, I. Koren, N. Lagrosas, P. Lestari, Z. Ma, J. Vanderlei Martins, E. J. Quel, Y. Rudich, A. Salam, S. N. Tripathi, C. Yu, Q. Zhang, Y. Zhang, M. Brauer, A. Cohen, M. D. Gibson, Y. Liu, Spartan: A global network to evaluate and enhance satellite-based estimates of ground-level particulate matter for global health applications. *Atmos. Meas. Tech.* **8**, 505–521 (2015).
37. C. L. Weagle, G. Snider, C. Li, A. van Donkelaar, S. Philip, P. Bissonnette, J. Burke, J. Jackson, R. Latimer, E. Stone, I. Abboud, C. Akoshile, N. X. Anh, J. R. Brook, A. Cohen, J. Dong, M. D. Gibson, D. Griffith, K. B. He, B. N. Holben, R. Kahn, C. A. Keller, J. S. Kim, N. Lagrosas, P. Lestari, Y. L. Khian, Y. Liu, E. A. Marais, J. V. Martins, A. Misra, U. Muliane, R. Pratiwi, E. J. Quel, A. Salam, L. Segev, S. N. Tripathi, C. Wang, Q. Zhang, M. Brauer, Y. Rudich, R. V. Martin, Global sources of fine particulate matter: Interpretation of $PM_{2.5}$ chemical composition observed by spartan using a global chemical transport model. *Environ. Sci. Technol.* **52**, 11670–11681 (2018).
38. S. Heft-Neal, J. Burney, E. Bendavid, M. Burke, Robust relationship between air quality and infant mortality in africa. *Nature* **559**, 254–258 (2018).
39. J. Proctor, S. Hsiang, J. Burney, M. Burke, W. Schlenker, Estimating global agricultural effects of geoengineering using volcanic eruptions. *Nature* **560**, 480–483 (2018).
40. M. Burke, S. M. Hsiang, E. Miguel, Global non-linear effect of temperature on economic production. *Nature* **527**, 235–239 (2015).
41. A. Stohl, S. Eckhardt, C. Forster, P. James, N. Spichtinger, On the pathways and timescales of intercontinental air pollution transport. *J. Geophys. Res. Atmos.* **107**, ACH 6-1–ACH 6-17 (2002).
42. D. T. Shindell, H. Teich, M. Chin, F. Dentener, R. M. Doherty, G. Faluvegi, A. M. Fiore, P. Hess, I. A. Mackenzie, M. G. Sanderson, M. G. Schultz, M. Schulz, D. S. Stevenson, C. Textor, O. Wild, D. J. Bergmann, H. Bian, C. Cuvelier, B. N. Duncan, G. Folberth, L. W. Horowitz, J. Jonson, J. W. Kaminski, E. Marmer, R. Park, K. J. Pringle, S. Schroeder, S. Laval-Szopa, T. Takemura, G. Zeng, T. J. Keating, A. Zuber, A multi-model assessment of pollution transport to the Arctic. *Atmos. Chem. Phys.* **8**, 5353–5372 (2008).
43. I. M. Held, B. J. Soden, Robust responses of the hydrological cycle to global warming. *J. Climate* **19**, 5686–5699 (2006).
44. Institute for Health Metrics and Evaluation, GBD Compare data visualization (2017).
45. M. L. Bell, K. Ebisu, K. Belanger, Ambient air pollution and low birth weight in Connecticut and Massachusetts. *Environ. Health Perspect.* **115**, 1118–1124 (2007).
46. D. P. Pope, V. Mishra, L. Thompson, A. R. Siddiqui, E. A. Rehfuess, M. Weber, N. G. Bruce, Risk of low birth weight and stillbirth associated with indoor air pollution from solid fuel use in developing countries. *Epidemiol. Rev.* **32**, 70–81 (2010).
47. W. Schlenker, D. B. Lobell, Robust negative impacts of climate change on African agriculture. *Environ. Res. Lett.* **5**, 014010 (2010).
48. A. Dechezleprêtre, N. Rivers, B. Stadler, "The economic cost of air pollution: Evidence from Europe" (OECD Economics Department Working Papers, No. 1584, OECD Publishing, 2019).
49. M. Kotz, A. Levermann, L. Wenz, The effect of rainfall changes on economic production. *Nature* **601**, 223–227 (2022).
50. European Commission and Joint Research Centre (JRC) and Netherlands Environmental Assessment Agency (PBL), Emission Database for Global Atmospheric Research (EDGAR), release version 4.2 (2012).
51. U. N. FAO, Food and Agriculture Organization of the United Nations statistical database (FAOSTAT) (accessed 2019).
52. W. K. Viscusi, C. J. Masterman, Income elasticities and global values of a statistical life. *J. Benefit Cost Anal.* **8**, 226–250 (2017).
53. L. A. Robinson, J. K. Hammitt, L. O'Keeffe, Valuing mortality risk reductions in global benefit-cost analysis. *J. Benefit Cost Anal.* **10**, 15–50 (2019).
54. U.S. Environmental Protection Agency (EPA), Mortality Risk Valuation (EPA, 2019).
55. Climate Action Tracker, Country target updates (2022); https://climateactiontracker.org/climate-target-update-tracker/.
56. N. Höhne, M. Den Elzen, D. Escalante, Regional ghg reduction targets based on effort sharing: A comparison of studies. *Clim. Policy* **14**, 122–147 (2014).

57. S. Rao, Z. Klimont, S. J. Smith, R. van Dingenen, F. Dentener, L. Bouwman, K. Riahi, M. Amann, B. L. Bodirsky, D. P. van Vuuren, L. Aleluia Reis, K. Calvin, L. Drouet, O. Fricko, S. Fujimori, D. Gernaat, P. Havlik, M. Harmsen, T. Hasegawa, C. Heyes, J. Hilaire, G. Luderer, T. Masui, E. Stehfest, J. Strefler, S. van der Sluis, M. Tavoni, Future air pollution in the Shared Socioeconomic Pathways. *Glob. Environ. Chang.* **42**, 346–358 (2017).
58. J. A. Burney, C. F. Kennel, D. G. Victor, Getting serious about the new realities of global climate change. *Bull. At. Sci.* **69**, 49–57 (2013).
59. S. Aakre, S. Kallbekken, R. Van Dingenen, D. G. Victor, Incentives for small clubs of arctic countries to limit black carbon and methane emissions. *Nat. Clim. Chang.* **8**, 85–90 (2018).
60. R. Wang, S. Tao, Y. Balkanski, P. Ciais, O. Boucher, J. Liu, S. Piao, H. Shen, M. R. Vuolo, M. Valari, H. Chen, Y. Chen, A. Cozic, Y. Huang, B. Li, W. Li, G. Shen, B. Wang, Y. Zhang, Exposure to ambient black carbon derived from a unique inventory and high-resolution model. *Proc. Natl. Acad. Sci. U.S.A.* **111**, 2459–2463 (2014).
61. H. Gadhavi, K. Renuka, V. R. Kiran, A. Jayaraman, A. Stohl, Z. Klimont, G. Beig, Evaluation of black carbon emission inventories using a Lagrangian dispersion model–A case study over southern India. *Atmos. Chem. Phys.* **15**, 1447–1461 (2015).
62. T. S. Carter, C. L. Heald, J. L. Jimenez, P. Campuzano-Jost, Y. Kondo, N. Moteki, J. P. Schwarz, C. Wiedinmyer, A. S. Darmenov, A. M. da Silva, J. W. Kaiser, How emissions uncertainty influences the distribution and radiative impacts of smoke from fires in North America. *Atmos. Chem. Phys.* **20**, 2073–2097 (2020).
63. D. V. Spracklen, A. Rap, Natural aerosol–climate feedbacks suppressed by anthropogenic aerosol. *Geophys. Res. Lett.* **40**, 5316–5319 (2013).
64. K. S. Carslaw, L. A. Lee, C. L. Reddington, K. J. Pringle, A. Rap, P. M. Forster, G. W. Mann, D. V. Spracklen, M. T. Woodhouse, L. A. Regayre, J. R. Pierce, Large contribution of natural aerosols to uncertainty in indirect forcing. *Nature* **503**, 67–71 (2013).
65. K. S. Carslaw, O. Boucher, D. V. Spracklen, G. W. Mann, J. G. L. Rae, S. Woodward, M. Kulmala, A review of natural aerosol interactions and feedbacks within the Earth system. *Atmos. Chem. Phys.* **10**, 1701–1737 (2010).
66. K. S. Carslaw, H. Gordon, D. S. Hamilton, J. S. Johnson, L. A. Regayre, M. Yoshioka, K. J. Pringle, Aerosols in the pre-industrial atmosphere. *Curr. Clim. Change Rep.* **3**, 1–15 (2017).
67. B. C. O'Neill, E. Kriegler, K. L. Ebi, E. Kemp-Benedict, K. Riahi, D. S. Rothman, B. J. van Ruijven, D. P. van Vuuren, J. Birkmann, K. Kok, M. Levy, W. Solecki, The roads ahead: Narratives for shared socioeconomic pathways describing world futures in the 21st century. *Glob. Environ. Chang.* **42**, 169–180 (2015).
68. M. T. Lund, G. Myhre, B. H. Samset, Anthropogenic aerosol forcing under the Shared Socioeconomic Pathways. *Atmos. Chem. Phys.* **19**, 13827–13839 (2019).
69. J. Rogelj, S. Rao, D. L. McCollum, S. Pachauri, Z. Klimont, V. Krey, K. Riahi, Air-pollution emission ranges consistent with the representative concentration pathways. *Nat. Clim. Chang.* **4**, 446–450 (2014).
70. G. G. Persad, D. J. Paynter, Y. Ming, V. Ramaswamy, Competing atmospheric and surface-driven impacts of absorbing aerosols on the East Asian summertime climate. *J. Climate* **30**, 8929–8949 (2017).
71. J. Graff Zivin, M. Neidell, The impact of pollution on worker productivity. *Am. Econ. Rev.* **102**, 3652–3673 (2012).
72. P. Bharadwaj, M. Gibson, J. G. Zivin, C. Neilson, Gray matters: Fetal pollution exposure and human capital formation. *J. Assoc. Environ. Resour. Econ.* **4**, 505–542 (2017).
73. A. Knohl, D. D. Baldocchi, Effects of diffuse radiation on canopy gas exchange processes in a forest ecosystem. *J. Geophys. Res. Biogeo.* **113**, G02023 (2008).
74. A. Rap, C. E. Scott, C. L. Reddington, L. Mercado, R. J. Ellis, S. Garraway, M. J. Evans, D. J. Beerling, A. R. MacKenzie, C. N. Hewitt, D. V. Spracklen, Enhanced global primary production by biogenic aerosol via diffuse radiation fertilization. *Nat. Geosci.* **11**, 640–644 (2018).
75. K. S. Hemes, J. Verfaillie, D. D. Baldocchi, Wildfire-smoke aerosols lead to increased light use efficiency among agricultural and restored wetland land uses in California's Central Valley. *J. Geophys. Res. Biogeo.* **125**, e2019JG005380 (2020).
76. T. A. Carleton, S. M. Hsiang, Social and economic impacts of climate. *Science* **353**, aad9837 (2016).
77. S. M. Hsiang, K. C. Meng, M. A. Cane, Civil conflicts are associated with the global climate. *Nature* **476**, 438–441 (2011).
78. J.-F. Lamarque, T. C. Bond, V. Eyring, C. Granier, A. Heil, Z. Klimont, D. Lee, C. Liousse, A. Mieville, B. Owen, M. G. Schultz, D. Shindell, S. J. Smith, E. Stehfest, J. van Aardenne, O. R. Cooper, M. Kainuma, N. Mahowald, J. R. McConnell, V. Naik, K. Riahi, D. P. van Vuuren, Historical (1850–2000) gridded anthropogenic and biomass burning emissions of reactive gases and aerosols: Methodology and application. *Atmos. Chem. Phys.* **10**, 7017–7039 (2010).
79. T. Takemura, Distributions and climate effects of atmospheric aerosols from the preindustrial era to 2100 along representative concentration pathways (RCPS) simulated using the global aerosol model sprintars. *Atmos. Chem. Phys.* **12**, 11555–11572 (2012).
80. X. Liu, R. C. Easter, S. J. Ghan, R. Zaveri, P. Rasch, X. Shi, J. F. Lamarque, A. Gettelman, H. Morrison, F. Vitt, A. Conley, S. Park, R. Neale, C. Hannay, A. M. L. Ekman, P. Hess, N. Mahowald, W. Collins, M. J. Iacono, C. S. Bretherton, M. G. Flanner, D. Mitchell, Toward a minimal representation of aerosols in climate models: Description and evaluation in the Community Atmosphere Model CAM5. *Geosci. Model Dev.* **5**, 709–739 (2012).
81. S. J. Ghan, X. Liu, R. C. Easter, R. Zaveri, P. J. Rasch, J. H. Yoon, B. Eaton, Toward a minimal representation of aerosols in climate models: Comparative decomposition of aerosol direct, semidirect, and indirect radiative forcing. *J. Climate* **25**, 6461–6476 (2012).
82. A. G. Koutroulis, M. G. Grillakis, I. K. Tsanis, L. Papadimitriou, Evaluation of precipitation and temperature simulation performance of the CMIP3 and CMIP5 historical experiments. *Climate Dynam.* **47**, 1881–1898 (2016).
83. G. Myhre, P. M. Forster, B. H. Samset, Ø. Hodnebrog, J. Sillmann, S. G. Aalbergsjø, T. Andrews, O. Boucher, G. Faluvegi, D. Fläschner, T. Iversen, M. Kasoar, V. Kharin, J.-F. Lamarque, D. Olivié, T. Richardson, D. Shindell, K. P. Shine, C. W. Stjern, T. Takemura, A. Voulgarakis, F. Zwiers, PDRMIP: A precipitation driver and response model intercomparison project–protocol and preliminary results. *Bull. Am. Meteorol. Soc.* **98**, 1185–1198 (2017).
84. W. J. Collins, J. F. Lamarque, M. Schulz, O. Boucher, V. Eyring, I. M. Hegglin, A. Maycock, G. Myhre, M. Prather, D. Shindell, J. S. Smith, AerChemMIP: Quantifying the effects of chemistry and aerosols in CMIP6. *Geosci. Model Dev.* **10**, 585–607 (2017).
85. G. He, M. Fan, M. Zhou, The effect of air pollution on mortality in China: Evidence from the 2008 Beijing Olympic Games. *J. Environ. Econ. Manage.* **79**, 18–39 (2016).
86. E. Arceo, R. Hanna, P. Oliva, Does the effect of pollution on infant mortality differ between developing and developed countries? Evidence from Mexico City. *Econ. J.* **126**, 257–280 (2016).
87. K. Y. Chay, M. Greenstone, The impact of air pollution on infant mortality: Evidence from geographic variation in pollution shocks induced by a recession. *Q. J. Econ.* **118**, 1121–1167 (2003).
88. Center for International Earth Science Information Network - CIESIN - Columbia University, Poverty Mapping Project: Global Subnational Infant Mortality Rates (2015).
89. Center for International Earth Science Information Network - CIESIN - Columbia University, Gridded Population of the World, Version 4 (GPWv4): Population Count, Revision 11 (2018).
90. R. Burnett, H. Chen, M. Szyszkowicz, N. Fann, B. Hubbell, C. A. Pope III, J. S. Apte, M. Brauer, A. Cohen, S. Weichenthal, J. Coggins, Q. di, B. Brunekreef, J. Frostad, S. S. Lim, H. Kan, K. D. Walker, G. D. Thurston, R. B. Hayes, C. C. Lim, M. C. Turner, M. Jerrett, D. Krewski, S. M. Gapstur, W. R. Diver, B. Ostro, D. Goldberg, D. L. Crouse, R. V. Martin, P. Peters, L. Pinault, M. Tjepkema, A. van Donkelaar, P. J. Villeneuve, A. B. Miller, P. Yin, M. Zhou, L. Wang, N. A. H. Janssen, M. Marra, R. W. Atkinson, H. Tsang, T. Quoc Thach, J. B. Cannon, R. T. Allen, J. E. Hart, F. Laden, G. Cesaroni, F. Forastiere, G. Weinmayr, A. Jaensch, G. Nagel, H. Concin, J. V. Spadaro, Global estimates of mortality associated with long-term exposure to outdoor fine particulate matter. *Proc. Natl. Acad. Sci. U.S.A.* **115**, 9592–9597 (2018).
91. A. J. Cohen, M. Brauer, R. Burnett, H. R. Anderson, J. Frostad, K. Estep, K. Balakrishnan, B. Brunekreef, L. Dandona, R. Dandona, V. Feigin, G. Freedman, B. Hubbell, A. Jobling, H. Kan, L. Knibbs, Y. Liu, R. Martin, L. Morawska, C. A. Pope III, H. Shin, K. Straif, G. Shaddick, M. Thomas, R. van Dingenen, A. van Donkelaar, T. Vos, C. J. L. Murray, M. H. Forouzanfar, Estimates and 25-year trends of the global burden of disease attributable to ambient air pollution: An analysis of data from the global burden of diseases study 2015. *Lancet* **389**, 1907–1918 (2017).
92. R. T. Burnett, C. A. Pope III, M. Ezzati, C. Olives, S. S. Lim, S. Mehta, H. H. Shin, G. Singh, B. Hubbell, M. Brauer, H. R. Anderson, K. R. Smith, J. R. Balmes, N. G. Bruce, H. Kan, F. Laden, A. Prüss-Ustün, M. C. Turner, S. M. Gapstur, W. R. Diver, A. Cohen, An integrated risk function for estimating the global burden of disease attributable to ambient fine particulate matter exposure. *Environ. Health Perspect.* **122**, 397–403 (2014).
93. C. Monfreda, N. Ramankutty, J. A. Foley, Farming the planet: 2. Geographic distribution of crop areas, yields, physiological types, and net primary production in the year 2000. *Global Biogeochem. Cycles* **22**, 3020791 (2008).
94. W. J. Sacks, D. Deryng, J. A. Foley, N. Ramankutty, Crop planting dates: An analysis of global patterns. *Glob. Ecol. Biogeogr.* **19**, 607–620 (2010).
95. Global Carbon Project, "Greenhouse gas emissions" (2022); www.globalcarbonproject.org/index.htm.
96. H. Lindhjem, S. Navrud, N. A. Braathen, V. Biausque, Valuing mortality risk reductions from environmental, transport, and health policies: A global meta-analysis of stated preference studies. *Risk Anal. An Int. J.* **31**, 1381–1407 (2011).

Acknowledgments

Funding: J.B., G.P., E.B., M.B., and S.H.-N. were supported by the National Science Foundation NSF CNH-L #1715557. **Author contributions:** All authors designed the research. G.P. designed and ran the climate simulations. J.B. analyzed the data with help from J.P. All authors wrote and revised the paper. **Competing interests:** The authors declare that they have no financial or other competing interests. **Data and materials availability:** All data needed to evaluate the conclusions in the paper are present in the paper and/or the Supplementary Materials. Underlying input emissions data files for the climate model runs are available at https://doi.org/10.18738/T8/Z87COZ; emissions perturbation scenario output data and other population, economic, and crop data are available at https://doi.org/10.7910/DVN/PLEYEF. Analysis code is available with the climate model output data at https://doi.org/10.7910/DVN/PLEYEF.

Submitted 15 December 2021
Accepted 9 August 2022
Published 23 September 2022
10.1126/sciadv.abn7307